

Elastic pd scattering with 200–300 MeV protons

H. Rohdjeß,^{1,*} W. Scobel,¹ H. O. Meyer,² P. V. Pancella,³ S. F. Pate,^{2,†} M. A. Pickar,⁴ R. E. Pollock,² B. v. Przewoski,² T. Rinckel,² F. Sperisen,² H. Witała,⁵ J. Golak,⁵ D. Hüber,⁶ H. Kamada,⁶ and W. Glöckle⁶

¹*Institut für Experimentalphysik, Universität Hamburg, D-22761 Hamburg, Germany*

²*Department of Physics, Indiana University, Bloomington, Indiana 47405*

³*Western Michigan University, Kalamazoo, Michigan 49008*

⁴*Department of Physics & Astronomy, Mankato State University, Mankato, Minnesota 56002*

⁵*Institute of Physics, Jagellonian University, Reymonta 4, PL-30059 Cracow, Poland*

⁶*Institut für Theoretische Physik II, Ruhr-Universität Bochum, D-44780 Bochum, Germany*

(Received 3 December 1997)

We have measured the pd elastic scattering with an electron-cooled beam of a proton storage ring and an internal jet target operated with HD gas. The accurately known H/D ratio is used to transfer the precision of existing pp scattering data to the pd cross sections. Measurements were performed for proton energies between 200 and 300 MeV in the angular range $11^\circ \leq \Theta_{\text{c.m.}} \leq 29^\circ$. The results are compared to nonrelativistic Faddeev calculations with different nucleon-nucleon interactions and total angular momenta $j \leq 5$ in the NN subsystem. The impact of a genuine $3N$ force is investigated. The discrepancies between data and calculations increase with projectile energy. [S0556-2813(98)04805-5]

PACS number(s): 25.10.+s, 21.30.-x, 21.45.+v, 25.40.Cm

I. INTRODUCTION

The advent of proton accelerators with cooled beams brings the study of the nucleon-nucleon (NN) interaction in few nucleon systems to unprecedented levels of precision in projectile energy and background suppression. By making use of polarized beams and/or internal gas targets these processes can be studied with polarization observables and near meson production thresholds.

For NN elastic scattering the database is sufficiently complete for projectile energies up to the pion production thresholds, and the existing phase shift analyses, e.g., [1,2], show only minor discrepancies due to spin observables that are not yet sufficiently represented in the database [3,4].

The situation is different for elastic pd scattering, where the data are scarce for $T_p \geq 150$ MeV and not at all comparable with that for NN . Elastic pd scattering represents a well-defined three nucleon problem and the angular distributions are of general interest as a test of calculations investigating the reaction mechanism. Rigorous solutions of the three-nucleon ($3N$) Faddeev equations for several types of realistic NN potentials have been derived [5,6], and many $3N$ observables for projectile energies below 100 MeV are described well by these potentials, see e.g., [7]. The $3N$ system thus provides the environment for tests of NN interactions in the presence of an additional nucleon. Faddeev calculations of elastic pd scattering can be performed for energies T_p beyond 150 MeV [7], and adequate NN force parametrizations exist for energies up to 350 MeV. Precision

measurements of elastic pd scattering test the predictive power of the Faddeev results for absolute values as well as for the dependence on angle and projectile energy. Furthermore the contributions attributed to higher total angular momenta in the NN subsystem and the impact of an additional genuine $3N$ force can be studied [7–11].

There is growing interest in pd elastic scattering data for normalization of inelastic pd reactions to absolute values, too. Indeed, pion production in the pd system has recently attracted much interest [4,12–16], because it can be approached as a fundamental NN interaction in a simple nuclear environment and represents the gateway to an understanding of meson production in nuclei. With appropriate corrections for the Fermi momentum distribution, the deuteron may also serve as an effective neutron target [17]. These experiments mostly focus on the projectile energies close above the meson production thresholds which are about 210 MeV for pion production. Absolute excitation functions can then be obtained by a normalization to simultaneously measured elastic scattering. This normalization technique has been frequently used for inelastic NN processes by making use of the existing precise database for elastic scattering. Recently the study of the reaction $pp \rightarrow pp\pi^0$ [18,19] has revealed that important and unexpected insight into the reaction dynamics is derived from the precise knowledge of *absolute* cross sections [20–22].

Such normalization cannot yet be applied to the pd system because elastic scattering cross sections for energies above the pion production threshold and forward angles are not available. There exist only a few data points for $T_p = 198$ MeV [23] and $T_d = 433$ MeV [24] for backward scattered protons, and for $T_p = 240$ MeV [25] covering $\Theta_{\text{lab}} = 21^\circ - 100^\circ$. For $T_p = 641$ MeV and 793 MeV measurements have been performed at a 5% precision level for angles $\Theta_{\text{c.m.}} \geq 35^\circ$ [26]. The idea of the present work is to transfer the accurately known absolute cross sections of pp

*Present address: ISKP, Universität Bonn, D-53115 Bonn, Germany.

†Present address: Department of Physics, New Mexico State University, Las Cruces NM 88003.

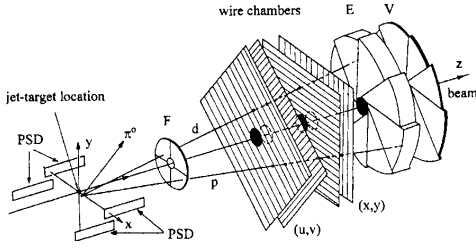


FIG. 1. Schematic drawing of the experimental setup. The components are described in the text. The trajectories of a $pd \rightarrow pd\pi^0$ event are shown, too.

elastic scattering to the pd elastic scattering just as it is done for the inelastic NN channels: We relate pd to elastic pp scattering with concurrent measurements of both reactions under identical conditions by using a high quality circulating proton beam in conjunction with an internal gas target. We present experimental results for pd elastic scattering in the forward angular range $9^\circ \leq \Theta_{\text{c.m.}} \leq 30^\circ$ with projectile energies $T_p = 200, 221, 235, 258,$ and 295 MeV relevant for pd reactions near pion thresholds.

Our paper is organized as follows. Section II is devoted to a description of the detector and the measurements; in Sec. III we present the experimental results and compare them to Faddeev calculations based on different choices for the NN potential without and with a $3N$ contribution. Our results are summarized in Sec. IV.

II. EXPERIMENTAL

The experiment was performed at the Cooler Ring [27] of the Indiana University Cyclotron Facility. The electron-cooled proton beam interacts with the perpendicular jet of an internal, windowless gas target. The target operates with a flow rate of more than 10^{19} molecules/s that pass through a 0.11 mm diameter Laval nozzle cooled to 40 K. In the nominal vertex region the target consists of a jet with a width of 3.3 mm (FWHM) and a background component distributed 8 cm up- and downstream along the beam path, resulting in an area density of about 1×10^{15} nuclei/cm². Beam currents are typically ≤ 100 μA and beam life times 50 s yielding time-averaged luminosities of 5×10^{29} cm⁻² s⁻¹.

It is essential for the experiment to run the target with a gas mixture that guarantees a known and stable ratio of the luminosities for interactions with its p and d contents, respectively. A mere mixture of H_2 and D_2 of known H_2/D_2 ratio was considered insufficient, because this ratio will vary along and across the gas jet and along the beam path due to the different molecular masses and flow dynamics. Therefore the target operates with HD gas that can provide this stable ratio. For confirmation, mass spectroscopical analyses have been performed prior to and after the experiment. They yielded the composition HD: H_2 : D_2 of initially 975:15:10 that, by dissociation and recombination under pressure, reduced to 971:17:12 within a month, resulting in an average H/D ratio of 1.0076 ± 0.0012 . In addition, the target was operated with pure H_2 and D_2 gas, respectively, for calibration purposes.

The setup (Fig. 1) is designed for detection of charged particles leaving the interaction region in the forward cone

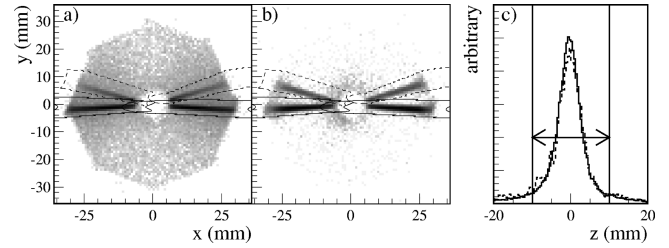


FIG. 2. Distribution of the intercept of the forward prong in the xy -wire chamber plane for (a) the D_2 and (b) the H_2 target. The gray code covers two orders of magnitude in logarithmic scaling. The cuts applied to events with a coincident signal from a PSD above (below) the horizontal plane are shown as solid (dashed) lines. (c) Gate on the scattering vertex position z along the beam path applied to elastic pd (solid histogram) and pp (dashed) scattering events. The gas jet is centered at $z = 0$.

$2^\circ \leq \Theta_{1,\text{lab}} \leq 19^\circ$; the acceptance is limited by the rim of the exit window on the outside, and inside by the beam pipe intersecting the detector. The detector stack is composed of five sensitive layers across the beam. The fourfold segmented F detector made from plastic scintillator NE102A of 0.5 mm thickness generates start signals for time-of-flight (TOF) measurements. Two subsequent pairs (u,v) and (x,y) of wire chambers each provide two-dimensional position information for vertex reconstruction. The eight segments of the E detector (10 cm thickness of plastic scintillator BC408) stop both protons and deuterons with energies up to 120 MeV and 160 MeV, e.g., from pion producing pd reactions, whereas elastically scattered protons or their deuteron recoils reach the scintillator segments labeled V. Further details on these detector components are given in [13,18,28].

Due to the composition of the HD target gas, the detector receives forward going protons from elastic pp and pd scattering; they carry almost the same energy and cannot be distinguished in the forward detector. The proton and deuteron recoils, however, differ in energy for a given forward proton angle sufficiently to enable a clean separation when measured in coincidence with good energy and position resolution. For this purpose, four position-sensitive silicon detectors (PSDs) of dimensions 45×8 mm² and 1000 μm thickness were mounted inside the same section of the reaction chamber as the gas jet target. Two of them were placed on each side of and about 12 cm away from the beam. On each side one was mounted 6 mm above the horizontal plane where the recoil deuterons from the gas jet position are expected, the other one 3 cm below the plane, further upstream along the beam and with maximum efficiency for recoil deuterons from the uniform gas distribution surrounding the gas jet. The position response of each PSD was calibrated by irradiation with α particles impinging on the detector through an aperture with equidistant slits.

The signature for elastic pp and pd events then is a forward proton generating signals in all 5 detector layers in coincidence with a PSD signal from the recoil. In addition cuts were applied to the data with gates for kinematically correct time differences. The resulting distribution of the prongs in the xy -wire chamber plane for forward going protons is shown in Fig. 2(b) for a pure H_2 gas jet. The four loci, one for each PSD, clearly stand out. A gate for each of them, shown as a solid (dashed) line for a PSD above (below) the horizontal plane, is applied to select the elastic scat-

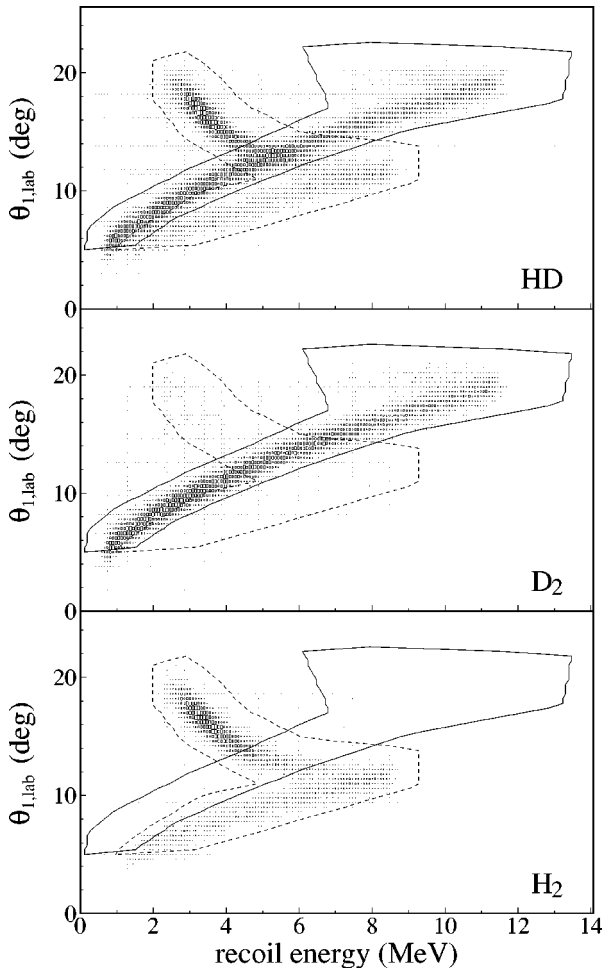


FIG. 3. Correlation plot of the proton angle $\Theta_{1,\text{lab}}$ vs energy loss of the recoil in the PSD at $T_p=200$ MeV obtained with the HD (top), the D₂, and the H₂ target, respectively. The gates mark deuteron (solid line) and proton (dashed) recoil candidates. With the HD target, two loci are seen.

tering candidates. There is little background, mostly close to the central hole for the beam pipe. Obviously the coincidence removes most of the background due to a beam halo or small angle scattering upstream the target region.

The corresponding distribution is shown in Fig. 2(a) for a pure D₂ gas jet. There is substantially more background outside the gates for coplanar PSD signals than for the H₂ target with a maximum for coplanar correlation. This background is attributed to deuteron breakup and quasifree pp scattering on deuteron target nuclei. Its subtraction is mandatory for measurements with the HD gas jet; it requires the discrimination of the recoil protons against deuterons in the PSD. This identification of the recoil particle in the PSD and the distinction of pp from pd scattering are based on the angular resolution of the wire chambers ($\Delta\Theta_{1,\text{lab}} < 1^\circ$) in conjunction with the energy information from the PSDs ($< 2\%$ FWHM). Protons (deuterons) up to 9 MeV (12 MeV) are stopped in the PSD, whereas recoils of higher energy deposit only the fraction corresponding to their stopping power. Figure 3 shows the kinematic loci that can be attributed to protons and deuterons, respectively, together with the gates to separate them. In the region where the gates overlap, a single event cannot be identified as either pp or pd . A subtraction

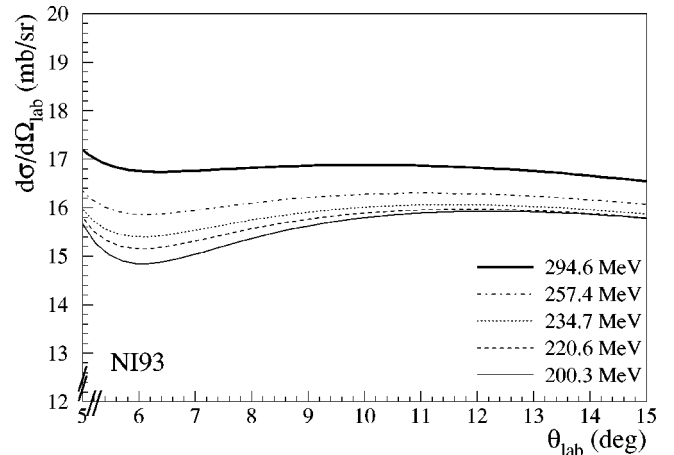


FIG. 4. Differential cross sections for pp elastic scattering from the solution (NI93) of Ref. [1] used to deduce the absolute cross section values of this work for pd elastic scattering. Note the suppressed zero on each axis.

has rather to be carried out on the spectra that are used as input to the calculation of the cross section by making use of the supplementary measurements with H₂ and D₂ gas jets.

The normalization of pd to pp scattering requires that the luminosities be the same for both event types, and so must the acceptances of the PSDs. The acceptance, however, varies with the vertex position z along the beam path. The vertex distribution in z can be reconstructed from the forward scattering angle $\Theta_{1,\text{lab}}$, the PSD information and the kinematical relation $\Theta_2(\Theta_{1,\text{lab}})$ for the recoil angle Θ_2 . Figure 2(c) shows the coinciding differential luminosity distributions for pp and pd events from the HD target, and the gate around the jet position at $z=0$ defining the accepted events. The subtraction procedure then starts from the distribution of events for the proton and deuteron gates in the z vs $\Theta_{1,\text{lab}}$ plane binned into $\Delta z=0.4$ mm and $\Delta\Theta_{1,\text{lab}}=0.4^\circ$ intervals, each for the H₂, the D₂, and the HD target. The determination of the final ratios of pp to pd scattering is restricted to a gate $z(\Theta_{1,\text{lab}})$ of vertex positions that is well within the acceptance of the PSDs for both pp and pd scattering.

The ratios of pp to pd scattering yields for corresponding solid angles, corrected with the known H/D ratio, were finally converted into differential pd scattering cross sections. For this purpose the data obtained from the two PSDs viewing the HD gas jet target have been combined. The pp differential cross sections are extracted from the Nijmegen phase shift analysis [1] based on pp and pn data below 350 MeV. The angular distributions resulting from this solution (NI93) are shown in Fig. 4 for reference purposes; they give a better fit to the experimental data in the angular range of our experiment than the older solution used in [13,28] as normalization reference. Our normalization is based on the integral from 6° – 11° ; the pd cross sections may be scaled to any new solution or source of pp scattering data.

III. DISCUSSION

A. Experimental results

The pd angular distributions are shown in Fig. 5 for the five energies under study. The error bars include contribu-

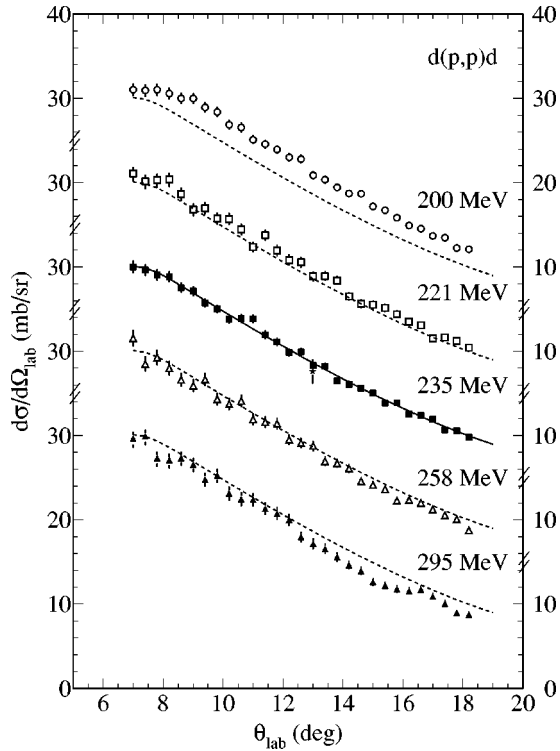


FIG. 5. Angular distributions of pd elastic scattering measured for the projectile energies T_p indicated. The overall normalization error δ_N of 5–8% is not included in the error bars. The solid line for the 235 MeV data is to guide the eye; it is shown as a dashed line for all other energies, too, to visualize the dependence on T_p . The datum from [25] for $T_p = 240$ MeV is shown (\star) with the 235 MeV data.

tions of comparable size from statistics, from variations of the gates on protons and deuterons (Fig. 3), from the event distribution along the beam [Fig. 2(c)], and from gain and position calibration factors of the PSDs. They are typically 3% or less. This figure, however, does not include the normalization uncertainty increasing from 3% (at $T_p = 200$ MeV) to 5% at 300 MeV; this number was estimated from the scatter of the experimental database around the solution NI93 chosen, and among the different phase shift analyses available in [1,2]. The pd cross section values are available in tabular form upon request [28].

The angular distributions exhibit a smooth energy dependence in absolute values as well as in their shape as may be seen in Fig. 5 by comparing them to the trend of the 235 MeV data (dashed lines). Figure 6 shows, that a major fraction of this dependence is removed by taking the squared momentum transfer q^2 instead of the scattering angle as variable. The cross sections $\sigma(T_p, \Theta)$ are available upon request.

In the angular and energy range under study only one partly overlapping angular distribution is available for comparison [25] that is in reasonable agreement with our results, see Fig. 5. In addition the backward angular range has been covered at $T_p = 198$ MeV [23] and $T_p = 216.5$ MeV [24]; these data will be included in the subsequent comparison with Faddeev calculations.

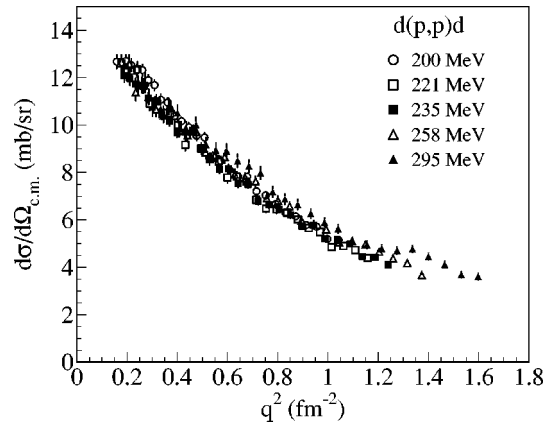


FIG. 6. The angular distributions of this work plotted as function of the squared momentum transfer q^2 .

B. Faddeev calculations

We compare our data to Faddeev calculations performed at the energies of the present experiment. Such calculations are now available with enough partial waves to be realistic at such high energies [7]. They are rigorous solutions of the $3N$ Faddeev equations based on modern, realistic NN interactions.

The transition operator U for elastic scattering is given in terms of the T operator for the breakup process

$$U = PG_0^{-1} + PT. \quad (1)$$

Here G_0 is the free $3N$ propagator and the permutation operator P consists of two parts, a cyclic and an anticyclic one, and accounts for the identity of the nucleons (we are working in isospin formalism). The matrix element of U between the initial state $|\phi\rangle$ and the corresponding final state determines the elastic scattering cross section. Those states are composed of the deuteron wave function and the momentum eigenstate of the free nucleon-deuteron motion.

The Faddeev equation for the T operator

$$T = tP + tPG_0T \quad (2)$$

sums up the multiple scattering series for three nucleons interacting through pairwise forces and propagating freely in between. The equation (2) is solved numerically for any given NN force. That NN force determines the two-nucleon off-shell t -matrix t by a Lippmann-Schwinger equation. For details of the theoretical formulation and the numerical performance we refer to Refs. [7,5,29,30].

In Figs. 7–9 we compare our data with Faddeev predictions using the CD Bonn NN potential [31]. At the high energies of the present experiment the “standard” calculations restricted to $2N$ force components (and the $3N$ partial waves) with total angular momenta of the two-nucleon subsystem $j \leq 3$ give an insufficiently convergent result for the elastic scattering angular distributions [7]. In order to demonstrate the importance of higher angular momenta components we show in Figs. 7 and 9 (for energies 200 MeV, 258 MeV, and 295 MeV, respectively) the theoretical predictions obtained by adding $j=4$ and $j=5$ force components. It is clear that the $j=4$ contribution significantly changes the the-

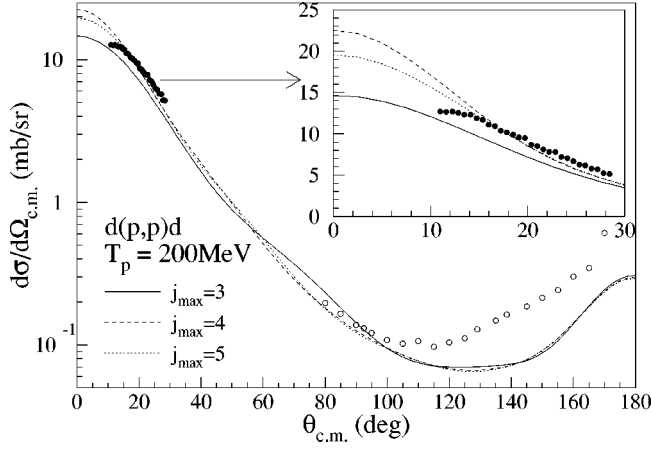


FIG. 7. Angular distributions. Solid symbols: This work ($T_p=200$ MeV); open symbols: Ref. [23] ($T_p=198$ MeV). The curves are the Faddeev results of the CD Bonn potential [31] for $j_{\max}=3, 4,$ and 5 . The inset shows the cross sections for $\Theta_{c.m.} \leq 30^\circ$ on a linear scale.

oretical cross sections while the influence of $j=5$ is restricted to forward angles $\Theta_{c.m.} < 10^\circ$. Terms with $j \geq 6$ are thus probably negligible. The theory underestimates the data at all angles by about 10% at 200 MeV and 20% at 295 MeV. The only exception is the very forward region of angles $\Theta_{c.m.} < 15^\circ$ at 200 MeV where, however, the Cou-

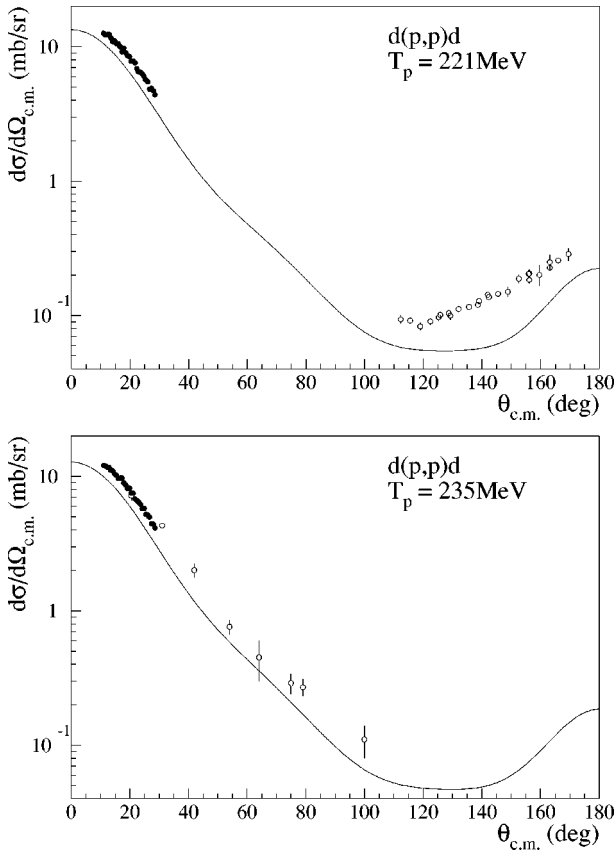


FIG. 8. Angular distributions. Top: Solid symbols, this work ($T_p=221$ MeV); open symbols, Ref. [24] ($T_p=433$ MeV). Bottom: Solid symbols, this work ($T_p=235$ MeV); open symbols, Ref. [25] ($T_p=240$ MeV). The curves are the results of the CD Bonn potential for $j_{\max}=3$.

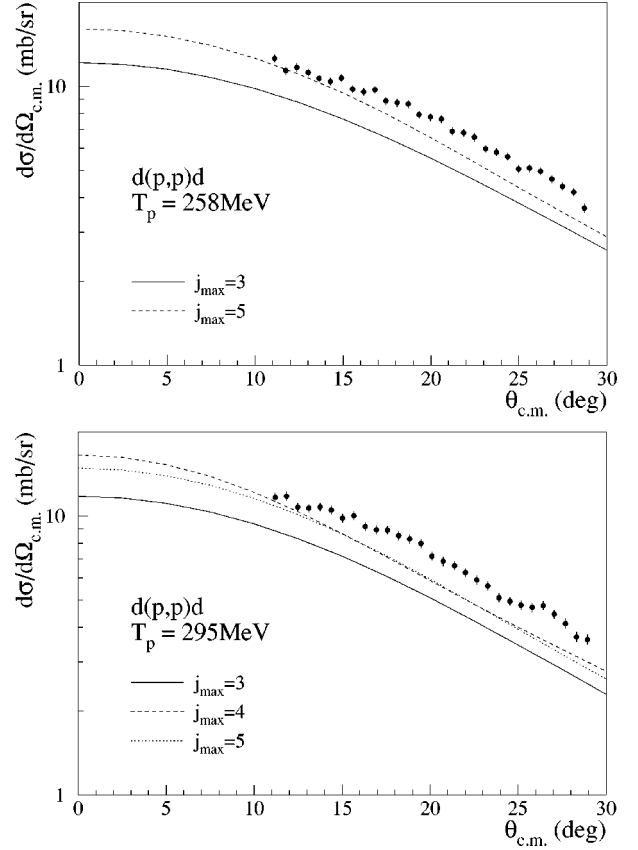


FIG. 9. Angular distributions. Solid symbols: This work (top: $T_p=258$ MeV; bottom: $T_p=295$ MeV); the curves are the results of the Bonn potential for $j_{\max}=3, 4$ and 5 .

lomb force between two protons, totally neglected in our 3N calculations, probably starts to become important and thus obscures our comparison. In fact an elastic p - ^4He calculation based on a full folding optical potential [40] shows very much the same bending at these smaller angles as we see in the data depicted in the inset to Fig. 7. When the Coulomb force is switched off in that calculation the curve behaves as our theoretical one for pd scattering. Therefore we can expect that Coulomb force effects should already be absent at about 20° .

In order to check for possible sources of this discrepancy we show in Fig. 10 the predictions at 200 MeV obtained with other modern NN interactions: AV18 [32] and NijmII [33]. In these calculations NN forces were restricted to $j \leq 3$ components. Differences between cross sections for those NN interactions are generally small and concentrated at angles $\Theta_{c.m.} > 90^\circ$. Results for the interaction NijmI [33] practically coincide with those for AV18 and are therefore not shown. Thus we can conclude that within the angular range under investigation there is no dependence on the NN potential chosen.

Another possibility is the action of a 3N force. As was shown in [34], the addition of a three nucleon force to the potential energy in the 3N Hamiltonian results in an elastic scattering transition operator U

$$U = PG_0^{-1} + P\tilde{T} + V_4^{(1)}(1+P) + V_4^{(1)}(1+P)G_0\tilde{T}, \quad (3)$$

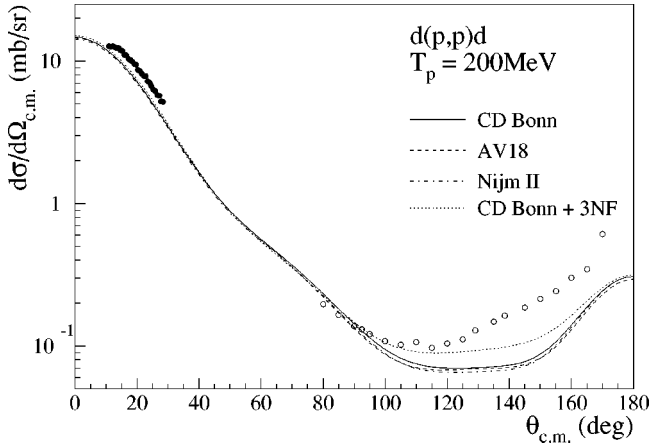


FIG. 10. Angular distributions. Solid symbols: This work ($T_p=200$ MeV); open symbols: Ref. [23] ($T_p=198$ MeV). The four curves are the results for the NN potentials: CD Bonn [31] (solid line), AV18 [32] (dashed), and Nijm [33] (dash-dotted), and for CD Bonn [31] with a $3N$ force added (dotted).

where the \tilde{T} operator fulfills the following equation:

$$\begin{aligned} \tilde{T} = & tP + (1+tG_0)V_4^{(1)}(1+P) + tPG_0\tilde{T} \\ & + (1+tG_0)V_4^{(1)}(1+P)G_0\tilde{T}. \end{aligned} \quad (4)$$

In the above expressions $V_4^{(1)}$ is one of three parts of the $3N$ force which is symmetrical under exchange of two nucleons and the $3N$ force is given by

$$V_4 = \sum_{i=1}^3 V_4^{(i)}. \quad (5)$$

We took the Tucson-Melbourne π - π exchange $3N$ force [35] with the cutoff parameter of the πN form factor chosen in such a way that for each NN interaction used (AV18, CD Bonn, and NijmII) the binding energy of the ${}^3\text{H}$ was reproduced [36]. In Fig. 10 the resulting elastic scattering cross sections at 200 MeV are shown for one case when such a $3N$ force is added. The corresponding curves for AV18 and NijmII are almost identical and thus not shown. These predictions were also obtained under the restriction of $j \leq 3$. Therefore the effect of such a $3N$ force on the elastic scattering cross section does not depend on the particular NN potential used and is significant only in the angular region $\Theta_{\text{c.m.}} > 90^\circ$ where it can be as large as 30%. However, it should be pointed out that the large angular momenta components required by our pure $2N$ force calculation indicate that the results with $3NF$ included are not fully convergent.

The discrepancy between data and theory which increases with increasing energy possibly indicates relativistic effects not accounted for in our purely nonrelativistic framework. Kinematical corrections, however, do not explain the discrepancy to the data. One can evaluate the relativistic phase-space factor and relativistic current of the projectile in the zero momentum frame. This leads to an increase of the cross section in relation to the nonrelativistic one by 2% at 200 MeV and 3% at 300 MeV. Therefore the observed systematic deviations may indicate the onset of dynamical relativistic effects. The nonrelativistic Schrödinger equation or

the equivalent Faddeev form thereof has to be replaced by a relativistic form, such that the Hamiltonian transforms under Poincare transformations as the energy component of a four vector. This involves also the correct boost properties of the NN t matrices and the Wigner rotations of the spins. Formulations in the instant or the light front form exist [37], but have not yet been applied in realistic numerical studies. Another approach, the Bethe-Salpeter equation, has been applied up to now only to NN scattering [38]. The increase in complexity going to a three-body system has not yet been overcome. However for the $3N$ bound state a first calculation in the framework of the Gross equation appeared [39], a framework which is closely related to the Bethe-Salpeter equation. Progress along one or the other relativistic formulations is badly needed.

IV. SUMMARY

Elastic scattering of protons on deuterons has been measured for five projectile energies between 200 and 300 MeV and c.m.s. angles ranging from 11° to 29° . The data are intended to provide reference cross sections for measurements of pion production in the pd system close above threshold, where elastic cross sections have so far not been available, and for comparison with rigorous Faddeev calculations testing different NN interactions.

The experiment has been carried out with an electron-cooled beam in a storage ring, making use of an internal HD gas jet target to compare pd to pp scattering rates with identical luminosities. Elastic scattering was identified by the forward-going protons in coincidence with the recoiling protons or deuterons that were detected and discriminated by means of position-sensitive silicon detectors. The production runs were accompanied by measurements with pure H_2 and D_2 gas jet targets for calibration purposes and background studies.

Absolute pd scattering cross sections were obtained by normalization of the pp scattering rates to the solution of the Nijmegen phase shift analysis [1]. The combined statistical plus systematical uncertainties are typically 3%; this number does not include the estimated normalization uncertainty $\leq 5\%$ due to the pp cross section input.

Fully converged Faddeev calculations based on modern NN forces in a nonrelativistic framework have been performed. In the angular range studied experimentally the various NN force predictions coincide, but underestimate the data by up to 20% with a trend toward increasing discrepancy with increasing energy. Possible sources for these discrepancies are only touched upon. A major effort is needed to develop and apply a truly dynamical relativistic framework. In view of the present capability to solve the $3N$ Faddeev equations rigorously and therefore to get faithful predictions resulting from any NN force input, the need arises for high precision data. In that respect the total uncertainty in the present pd data of up to 6% is a substantial improvement over the situation for larger angles where few pd data exist; in addition the uncertainties in the latter are partly uncomfortably large and smaller error bars would sharpen the view on the nature of defects in the theory.

ACKNOWLEDGMENTS

We thank the operating team of the IUCF Cooler for excellent beam support. This work was supported by the German BMBF, contract 06HH852, by the U.S. NSF under

Grant No. PHY-9103794, and by the DFG (project G187/24-1). The numerical calculations have been performed on the Cray T90 of the Höchstleistungsrechenzentrum in Jülich, Germany.

-
- [1] V. G. J. Stoks, R. A. M. Klomp, M. C. M. Rentmeester, and J. J. de Swart, *Phys. Rev. C* **48**, 792 (1993).
- [2] R. A. Arndt, I. I. Strakovsky, and R. L. Workman, *Phys. Rev. C* **50**, 2731 (1994); the interactive *NN* database SAID, accessed by TELNET 128.173.176.61, login PHYSICS, password QUANTUM.
- [3] C. Lechanoine-LeLuc and F. Lehar, *Rev. Mod. Phys.* **65**, 1 (1993).
- [4] H. O. Meyer, *Annu. Rev. Nucl. Part. Sci.* **47**, 235 (1997).
- [5] H. Witała, T. Cornelius, and W. Glöckle, *Few-Body Syst.* **3**, 123 (1988).
- [6] D. Hüber, H. Witała, and W. Glöckle, *Few-Body Syst.* **14**, 171 (1993).
- [7] W. Glöckle, H. Witała, D. Hüber, H. Kamada, and J. Golak, *Phys. Rep.* **274**, 107 (1996).
- [8] W. Glöckle, H. Kamada, H. Witała, D. Hüber, and J. Golak, *Few-Body Syst., Suppl.* **8**, 9 (1996).
- [9] H. Witała, D. Hüber, W. Glöckle, J. Golak, A. Stadler, and J. Adam, Jr., *Phys. Rev. C* **52**, 1254 (1995).
- [10] D. Hüber, H. Witała, A. Nogga, W. Glöckle, and H. Kamada, *Few-Body Syst.* **22**, 107 (1997).
- [11] L. D. Knutson, in *Proceedings of the XVth International Conference on Few Body Problems in Physics, Groningen, The Netherlands, 1997*, edited by J. C. S. Baclear, A. E. L. Dieperink, and R. A. Malfliet (Elsevier Science, Amsterdam, The Netherlands, 1997), p. 9.
- [12] M. A. Pickar, A. D. Bacher, H. O. Meyer, R. E. Pollock, and G. T. Emery, *Phys. Rev. C* **46**, 397 (1992).
- [13] H. Rohdjeß *et al.*, *Phys. Rev. Lett.* **70**, 2864 (1993).
- [14] H. O. Meyer and J. A. Niskanen, *Phys. Rev. C* **47**, 2474 (1993).
- [15] G. Fäldt and C. Wilkin, *Phys. Lett. B* **382**, 209 (1996).
- [16] J. Greiff, I. Koch, H. Rohdjeß, and W. Scobel, *Acta Phys. Pol. B* **27**, 2965 (1996).
- [17] H. Calén *et al.*, *Phys. Rev. Lett.* **79**, 2642 (1997).
- [18] H. O. Meyer, C. Horowitz, H. Nann, P. V. Pancella, S. F. Pate, R. E. Pollock, B. von Przewoski, T. Rinckel, M. A. Ross, and F. Sperisen, *Nucl. Phys.* **A539**, 633 (1992).
- [19] A. Bondar *et al.*, *Phys. Lett. B* **356**, 8 (1995).
- [20] T. S. H. Lee and D. O. Riska, *Phys. Rev. Lett.* **70**, 2237 (1992).
- [21] T. D. Cohen, J. L. Friar, G. A. Miller, and U. van Kolck, *Phys. Rev. C* **53**, 2661 (1996); B. Y. Park, F. Myhrer, J. R. Morones, T. Meissner, and K. Kubodera, *ibid.* **53**, 1519 (1996).
- [22] T. Sato, T. S. H. Lee, F. Myhrer, and K. Kubodera, *Phys. Rev. C* **56**, 1246 (1997).
- [23] R. E. Adelberger and C. N. Brown, *Phys. Rev. D* **5**, 2139 (1972).
- [24] G. Igo, J. C. Fong, S. L. Verback, M. Goitein, D. L. Hendrie, J. C. Carroll, B. McDonald, A. Stetz, and M. C. Makino, *Nucl. Phys.* **A195**, 33 (1972).
- [25] R. D. Schamberger, *Phys. Rev.* **85**, 424 (1952).
- [26] E. Gülmez *et al.*, *Phys. Rev. C* **43**, 2067 (1991).
- [27] R. E. Pollock, *Annu. Rev. Nucl. Sci.* **41**, 357 (1991).
- [28] H. Rohdjeß, Ph.D. thesis, Universität Hamburg, 1994.
- [29] W. Glöckle, *The Quantum-Mechanical Few-Body Problem* (Springer-Verlag, Berlin-Heidelberg, 1983).
- [30] W. Glöckle, in *Models and Methods in Few-Body Physics*, edited by L. S. Ferreira, A. C. Fonseca, and L. Streit, *Lecture Notes in Physics*, Vol. 273 (Springer-Verlag, Berlin, 1987), p. 3.
- [31] R. Machleidt, F. Sammarruca, and Y. Song, *Phys. Rev. C* **53**, R1483 (1996).
- [32] R. B. Wiringa, V. G. J. Stoks, and R. Schiavilla, *Phys. Rev. C* **51**, 38 (1995).
- [33] V. G. J. Stoks, R. A. M. Klomp, C. P. F. Terheggen, and J. J. de Swart, *Phys. Rev. C* **49**, 2950 (1994).
- [34] D. Hüber, H. Kamada, H. Witała, and W. Glöckle, *Acta Phys. Pol. B* **28**, 1677 (1997).
- [35] S. A. Coon and W. Glöckle, *Phys. Rev. C* **23**, 1790 (1981).
- [36] A. Nogga, D. Hüber, H. Kamada, and W. Glöckle, *Phys. Lett. B* **409**, 19 (1997).
- [37] B. D. Keister and W. N. Polyzou, *Adv. Nucl. Phys.* **20**, 225 (1991).
- [38] J. A. Tjon, *Few-Body Syst., Suppl.* **1**, 444 (1986).
- [39] A. Stadler, in *Proceedings of the XVth International Conference on Few Body Problems in Physics*, [11], p. 152.
- [40] Ch. Elster, private communication.